

Observation of strong wavelength-shifting in the argon-tetrafluoromethane system

P. Amedo,^a D. González-Díaz,^a F. M. Brunbauer,^b D. J. Fernández-Posada,^a E. Oliveri,^b L. Ropelewski^b

^a*IGFAE, Universidade de Santiago de Compostela, Spain*

^b*CERN, Geneva, Switzerland*

E-mail: pablo.amedo.martinez@usc.es

ABSTRACT: We report the scintillation spectra of Ar/CF₄ mixtures in the range 210-800 nm, obtained under X-ray irradiation for various pressures (1-5 bar) and concentrations (0-100%). Special care was taken to eliminate effects related to space charge and charge recombination, so that results can be extrapolated following conventional wisdom to those expected for minimum ionizing particles under the typical electric fields employed in gaseous instrumentation. Our study sheds light into the microscopic pathways leading to scintillation in this family of mixtures and reinvigorates the prospects of use in next-generation scintillation-based chambers.

KEYWORDS: Gaseous detectors; Time projection Chambers; Scintillators, scintillation and light emission processes (solid, gas and liquid scintillators)

Contents

1	Introduction	1
2	Experimental setup	2
3	Results	6
3.1	Pure gases	6
3.2	Ar/CF ₄ mixtures	7
4	Discussion	9
4.1	Wavelength-shifting pathways	9
4.2	Comparison with previous results	15
5	Conclusions	16
A	Electric field in the ionization volume	21
B	Charge recombination	23
C	Gas mixing and calibration	25

1 Introduction

Since their introduction in 1974 [1], time projection chambers (TPCs) have proved to be one of the most effective ways of detecting particles and reconstructing their trajectories. The versatility of these devices, being compatible with B -fields, allowing readout flexibility and a wide range of density media (from some 10's of mbar up to 10's of bar, liquid or even solid phase), makes them the perfect tool to study many different phenomena in particle physics [2].

Gas-based TPCs commonly operate with admixtures of noble gases with some molecular species, chiefly CH₄, *i*-C₄H₁₀, CF₄ or CO₂. TPCs make use of these additives to reduce the spatial spread and collection time of the primary ionization, minimize photon and ion feedback and, in general, to attain a greater stability. Among them, CF₄ exhibits some particularly interesting properties such as intense and broadband scintillation in the range 150-750 nm under primary [3–5] and secondary (field-assisted) [6–8] particle excitation, and very low electron diffusion [9]. The VUV-visible scintillation yields induced by α particles in pure CF₄ are found in the range 1000-3000 ph/MeV [3, 5, 10, 11], optical gains well above 10⁴ have been reported in CF₄-based mixtures in [8], while diffusion coefficients have been shown to remain at the thermal limit up to pressure-reduced drift fields as high as 1 kV/cm/bar [9].

Based on the aforementioned observations, CF₄ by itself makes an interesting TPC gas (and has been used to that aim before, e.g. [12, 13]). In fact, CF₄ either pure or admixed with other elements is of great contemporary interest to the optical imaging of rare processes in low-pressure

gases [14, 15]. Ar/CF₄ admixtures, in particular, have been pioneered by the Fraga&Fraga group at Coimbra already in the 00's for optical imaging [16, 17], and revived recently in an optical-TPC demonstrator equipped with a triple-stack of gas electron multipliers (GEMs), [8, 18]. These works consistently showed a higher optical gain compared to pure CF₄, with indirect evidence for wavelength-shifting reactions between Ar states and the CF₄ scintillation precursors. Besides the enhanced performance of Ar/CF₄ mixtures for GEM operation, argon is considerably more cost-effective and environment-friendly than CF₄. Compared to a traditional wavelength-shifter like N₂, main advantages of CF₄ are its strong scintillation in the visible range together with a much lower electron diffusion, potentially allowing sharper and brighter tracks from CMOS and CCD cameras, e.g, when instrumenting optical TPCs in the field of nuclear physics [19, 20].

Argon has another characteristic relevant to modern instrumentation: it is the element of choice of the DUNE experiment, where it acts simultaneously as target and detection medium both at its far and near detector complexes [21]. Specifically, an argon-rich high pressure TPC capable of reconstructing low-energy hadrons (down to 10's of MeV, at least) has been proposed by the collaboration [22]. It is called to be the first detector to ever record neutrino interactions in a sparse medium, with 4π coverage and broad particle identification (PID) capabilities. In this context, enabling time-tagging through the primary scintillation produced in neutrino interactions, while preserving the argon medium as pure as possible (to avoid parasitic neutrino interactions), is the subject of ongoing investigations [23, 24]. Time tagging is an essential asset in the study of neutrino oscillations with TPCs as it is used for spill-assignment, absolute estimate of the drift distance and time-of-flight determination of the emerging particles [25].

With this in mind, we performed a systematic study of the primary scintillation in the Ar/CF₄ system down to trace-amounts of the molecular additive, in order to better understand its wavelength-shifting capabilities. For that, a spectroscopic analysis was carried out under X-ray irradiation at varying pressures and CF₄ concentrations, at electric fields and ionization densities for which space charge and charge/light recombination effects are negligible. Following conventional wisdom (e.g., [26, 27]), measurements in these conditions should represent a good approximation to the scintillation by minimum ionizing particles, a typical metric for characterizing the response of a particle detector. The present work is structured as follows: in section 2 the experimental setup and procedures are described, section 3 compiles the scintillation spectra of the pure gases and Ar/CF₄ admixtures; in section 4 we present a minimalistic kinetic model that describes the observations to good accuracy, and we finally end with a comparison with previous results and a summary of our main conclusions in 5.

2 Experimental setup

Figure 1 shows a schematic drawing of the experimental setup. Measurements were performed on a CF63 aluminum-cube serving as a vessel, irradiated with X-rays from a copper tube at 40 kV. The chamber had an entrance window of 1 cm-diameter made of a thin aluminum foil of 50 μm thickness which was facing the tube. Inside the chamber, an electrifiable cylindrical volume was placed, with 3 cm in diameter and 0.75 cm in height. Its upstream electrode served as a cathode and was made from the same foil as the window. A semitransparent Cr-mesh served as the anode, evaporated on top of a collimating lens (OceanOptics 74-UV) leading to a multi-mode optical fiber (UV-VIS, 600 μm core) and finally coupled to an OceanOptics FX UV-VIS CCD spectrometer sensitive in

the 210-800 nm range. The photon spectrometer was calibrated using a lamp with reference light sources for the UV and the visible regions, coupled to the anode mesh. Both calibrations were merged at around the 300 nm mark.

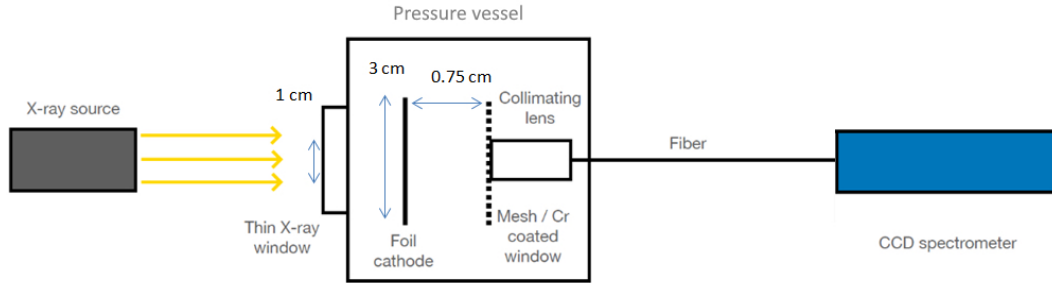


Figure 1. Schematic drawing of the experimental setup used to conduct the measurements. The x-ray tube is shown to the left, the high-pressure vessel housing the electrifiable scintillating cylinder is shown at the middle. The spectrophotometer is shown to the right.

Upon excitation and ionisation of the gas, electrons and ions were collected by means of an uniform electric field, the current being read at the anode with a Keithley picoamperemeter (model 6487). The maximum of the X-ray bremsstrahlung spectrum, when accounting for the absorption in the materials interposed up to the ionization region, was estimated to be at around 12 keV, a characteristic energy for which the X-ray mean free path is 14 cm in argon and 62 cm in CF₄, in standard conditions [28]. Even for argon at the highest pressures employed in our measurements (5 bar) the mean free path is as large as 2.8 cm, leading to $\pm 10\%$ -level variations within the ionization volume. The size of the ionization cloud (σ) caused by the tortuous trajectory of the ejected photoelectron amounts to a mere 0.25 mm/P[bar] in argon (see e.g. [29]), much smaller than the chamber dimensions. The additional spread stemming from electron diffusion along a 0.75 cm drift-path, when considering electric fields at full charge-collection, can increase the above figure up to 1.6 mm in the radial direction (Pyboltz, [30]). This situation corresponds to pure Ar at 1 bar, with other conditions involving yet smaller charge spreads by roughly a factor of $1/\sqrt{P}$ [bar] as the pressure increases, and up to another factor of ten as CF₄ concentration increases. Overall, inside the collimated region, ionization can be thus regarded as uniform throughout these measurements, for practical purposes.

To exclude space charge and charge-recombination effects, data was taken at no field and at a field high enough to guarantee full charge-collection (Fig. 2-left). Along this line, additional measurements were performed for different X-ray intensities too (e.g., Fig. 2-right). Under the assumption of uniform irradiation within the collimated region of the scintillation cell (of area $A = \pi * 0.5^2 \text{ cm}^2$), the positive-ion space-charge density ($q_e \cdot dN/dV|_{ion}$) relates to the steady-state current at full collection through:

$$I_{sst} = 2 \left(q_e \frac{dN}{dV} \right)_{ion} \cdot A \cdot \mu \cdot E \quad (2.1)$$

with q_e being the electron charge, μ the ion mobility,¹ E the electric field, and the factor 2 accounts

¹A discussion on the inputs to the ion mobilities is given in the appendix.

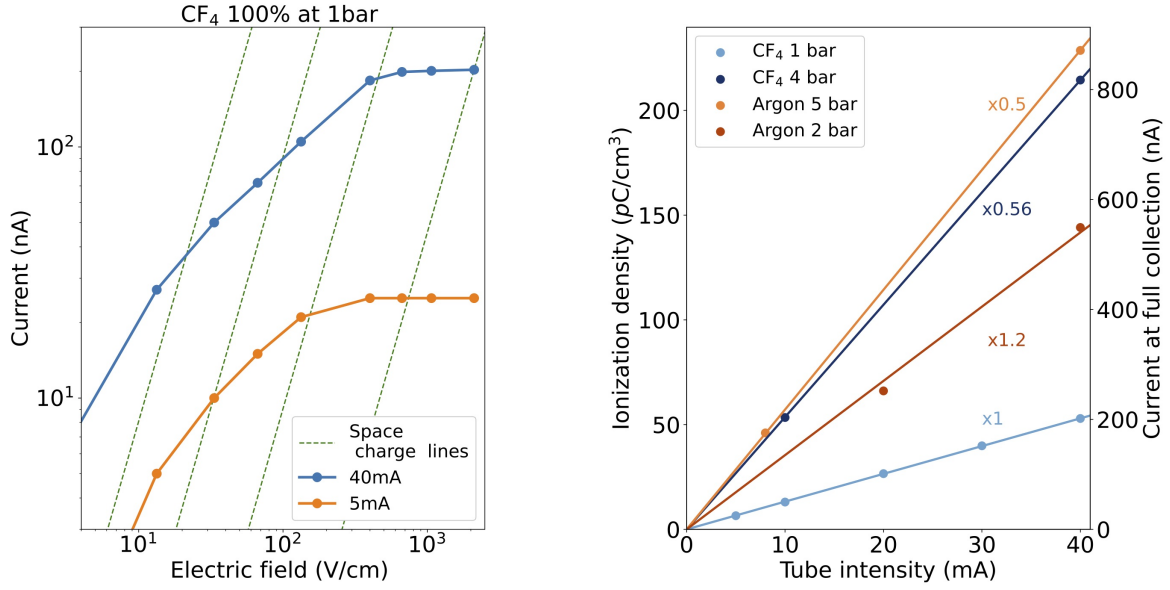


Figure 2. Exemplary scans in electric field and X-ray intensity. Left: current at the anode of the scintillation cell as a function of the applied electric field up to reaching full-collection, for different currents of the X-ray tube (pure CF₄ at 1 bar). Green lines represent identical space charge conditions (i.e., same degree of field distortion by positive ions) according to the parameter α introduced in [31] and discussed in section A of the appendix. Right: current at full charge-collection (right axis) and associated ionization density (left axis) as a function of the current of the X-ray tube for CF₄ at 1 and 4 bar (light and dark blue) and pure argon at 2 and 5 bar (red and orange). Each of them was fitted to a proportional trend. (Given the non-linear map between the current and the ionization density, each data series includes an additional multiplicative factor in order to transform the right-axis value into the correct one)

for the equal sharing of current between ions and electrons. Accordingly, the positive-ion space charge ranged in these measurements from 6 pC/cm³ (for pure CF₄ at around 1 bar and the lowest X-ray intensity) up to 225 pC/cm³ (for either pure Ar or CF₄ at around 5 bar, and the highest X-ray intensity). At 1 bar these values are about a factor of 4 below those employed in earlier measurements performed under α particles in [4], and reported to be recombination-free. Even the highest pressures explored in this work barely exceed the ionization densities studied earlier, which leads us to believe that recombination is negligible in present conditions. The good proportionality observed in Fig. 2-right for different intensities of the X-ray tube adds further support to this.²

In order to exclude any space charge effect from the positive ions, the analysis procedure sketched in [31] was applied. It follows, as discussed in appendix (section A), that field distortions once the current reached saturation (full collection) were typically at the 5%-level or below (with a maximum field distortion of 15%) during the measurements. The resulting iso-space-charge lines (green dashed, in Fig. 2-left) suggest that space charge is the main variable driving the current vs field behaviour. In the absence of space charge, the extent of fringe fields inside the chamber were evaluated through an electrostatic simulation. Results obtained with the COMSOL Multiphysics[®]

²A detailed argumentation on the absence of recombination in these measurements can be found in the appendix.

package [32] indicate that the field is uniform within the ionization region, for practical purposes.³

Prior to the measurements, the chamber was pumped down to 10^{-4} mbar. Ar/CF₄ mixtures were studied at a volume fraction of 100/0, 99.9/0.1, 99.8/0.2, 99.5/0.5, 99/1, 98/2, 95/5, 90/10 and 0/100, and pressures from 1 to 5 bar. The purity of the bottles was 4.5 (CF₄) and 6 (Ar), so the overall purity of the studied mixtures was between 5.5 and 6 (i.e., 1-3 ppm contamination). The chamber was first filled with CF₄ until the desired partial pressure, using two pressure/vacuum gauges, namely a Pfeiffer Vacuum PCR 280 Pirani/Capacitance and an MKS pressure transducer, for the readings. Afterwards, argon was admixed. Gas circulation was dimmed unnecessary for proper mixing, as the concentration could be verified by sampling the gas into a residual gas analyzer and waiting for the ratio of the pressures of the species to stabilize. This agrees with the notion that the forced flow of argon gas, being dominant by at least a factor 10 in volume, drives the mixing in such a small chamber. For the lowest CF₄ concentrations, that would be limited by the accuracy of the sensor, the filling was done at high pressure and diluted until the target concentration was achieved. Deviations from the target CF₄ concentrations [0, 0.1, 0.2, 0.5, 1, 2, 5, 10, 100]% were quantified through a linear fit and associated uncertainties. Although the target values will be used as plot descriptors in the following, the calibrated values will be used when presenting systematics as well as for model fitting.⁴

Purity was monitored continuously with a residual gas analyzer (RGA) coupled to the main system through a leak valve. The RGA region was kept at a constant pressure of 10^{-5} mbar throughout the measurements by adjusting the leak-valve opening. The main impurities in the system were H₂O, O₂ and N₂(CO) and their concentrations were estimated to be below 1000 H₂O ppm, 15 O₂ ppm and 200 N₂ ppm, being the sensitivity limited by the RGA background. These upper limits, as well as the scintillation yields, showed little variation with time, for a time span of hours. Even if we were to take them as representing the actual concentrations, it has been shown in [33] that N₂ concentrations as high as 4% are needed to quench CF₄ scintillation by a factor 2 (at 1 bar). Although 1000 ppms (0.1% per volume) might arguably compete with Ar-CF₄ transfers at about the same CF₄ concentration (the lowest one used in our measurements), the phenomenological model introduced later in text does not show any strong deviation for that case. These observations, together with the nominal purity of the bottles, the use of low-outgassing materials for chamber assembly and the stability of the scintillation yields with time, suggest that the impact of impurities is of little relevance to the results presented in this work.

The final scintillation spectrum was divided by the current at full collection, and by the average energy to create an electron-ion pair (W_I). The latter was taken from the directly-measured values in [34], except in the range [0-1]% CF₄ where a simple linear interpolation was used. An absolute normalization was not attempted and thus the spectrum is hereafter expressed in yield/eV [a.u.]. As no significant contribution from recombination or space charge was found in present data, the standard deviation of measurements performed for different X-ray intensities has been used to estimate the uncertainty. This accounts for any residual recombination effect as well as systematic errors that may be present in the measurements.

³For details on the electric field calculations, including space charge, the reader is referred to the appendix.

⁴For details on the calibration procedure, the reader is referred to the appendix.

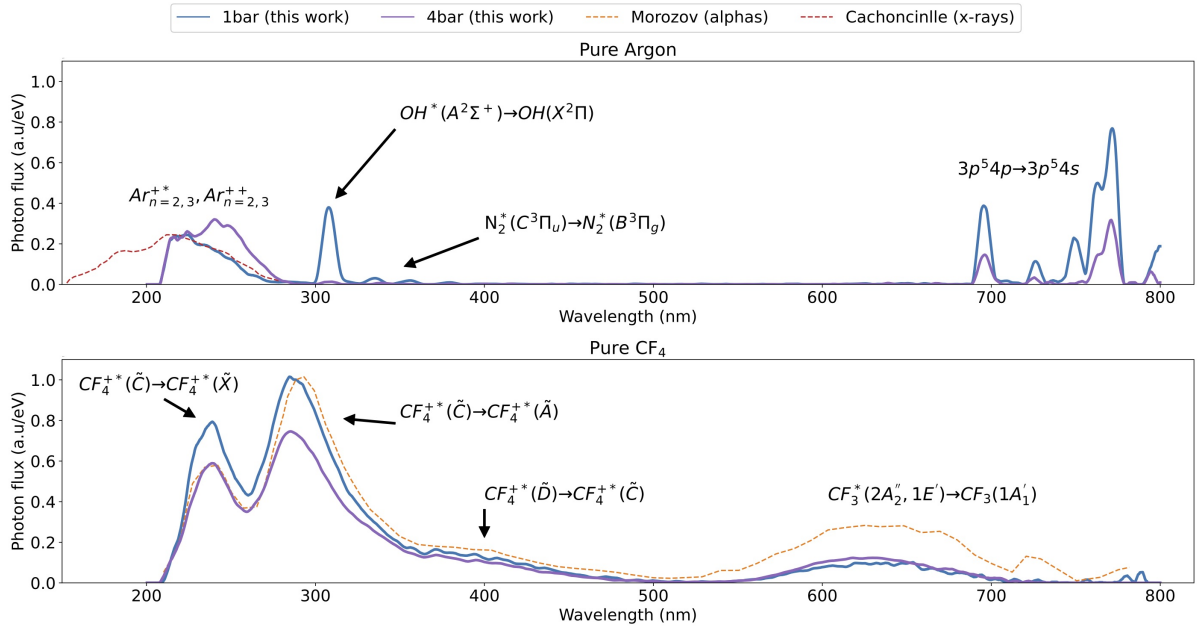


Figure 3. Emission spectra per eV of released energy for pure argon (upper plot) and pure CF₄ (lower plot) at 1 and 4 bar (blue, purple), obtained at zero field. No significant dependence with the intensity of the X-ray tube was observed, suggesting that measurements are recombination-free. For pure CF₄, where full charge-collection could be reached before the onset of secondary scintillation, no dependence with the electric field was observed either. The spectra of argon’s 3rd continuum obtained in [35] also with X-rays (red-dashed) and the one of CF₄ obtained in [3] with α -particles (orange-dashed) are shown for comparison. A global normalization was imposed by setting to 1 the maximum of the 290 nm peak in pure CF₄ at 1 bar.

3 Results

3.1 Pure gases

Figure 3 shows the scintillation spectra of Ar (top) and CF₄ (bottom) at pressures of 1 bar (blue) and 4 bar (purple). Bands that are easily identifiable are the ones of the 3rd continuum of argon (160-280 nm) [35] and the (210-500 nm) and (550-750 nm) ones of CF₄ [3]. The visible band centered at around 630 nm has been attributed earlier to the transition CF₃^{*}(2A₂'', 1E') \rightarrow CF₃(1A₁') [36–38] (not being assigned unequivocally to either the 2A₂'' or the 1E' states). The overlapping UV bands can be attributed to the CF₄^{+*} ion, emitting from its \tilde{C} , \tilde{D} states. Transitions $\tilde{C} \rightarrow \tilde{X}$, \tilde{A} can be naturally assigned to the peaks centered around 230 nm and 290 nm [39–41] while the transition at 364 nm may be assigned to $\tilde{D} \rightarrow \tilde{C}$. Another prominent UV band at around 260 nm has been observed before, e.g., under excitation within low-energy electron avalanches [6], and can be assigned to the transition CF₃^{*}(2A₁') \rightarrow CF₃(1A₂'') [36, 37]; it is however hidden in present conditions under the CF₄^{+*} emission. The small decrease of the yields in the UV bands as a function of pressure has been observed before in [3] and might be naturally attributed to self-quenching. A comparison with data from [3] obtained at 1 bar under α -particle irradiation is shown in Fig. 3 (orange, dashed), arbitrarily normalized to the 290 nm peak.

Concerning Ar, the 3rd continuum (cut by the spectrometer bandwidth below 210 nm) agrees

in shape with earlier X-ray measurements from [35], increasing the yield on its blue-wing as the pressure increases, qualitatively in agreement with that work too (red dashed-line). In the near-infrared region the main lines located at 696, 727, 750, 763 and 772 nm can be clearly identified, corresponding to transitions between the $3p^54p$ and $3p^54s$ multiplets [42]. Their associated yields seem to be dominated by 2-body collisional self-quenching, thus approximately following a $\sim 1/(a + bP)$ trend, except in the case of the 750 nm peak where a $\sim 1/(a + bP^2)$ trend is observed instead (Fig. 4). The strong suppression observed as a function of CF_4 concentration suggests that argon IR-yields will be subdominant in high pressure applications and/or as soon as a molecular additive is added.

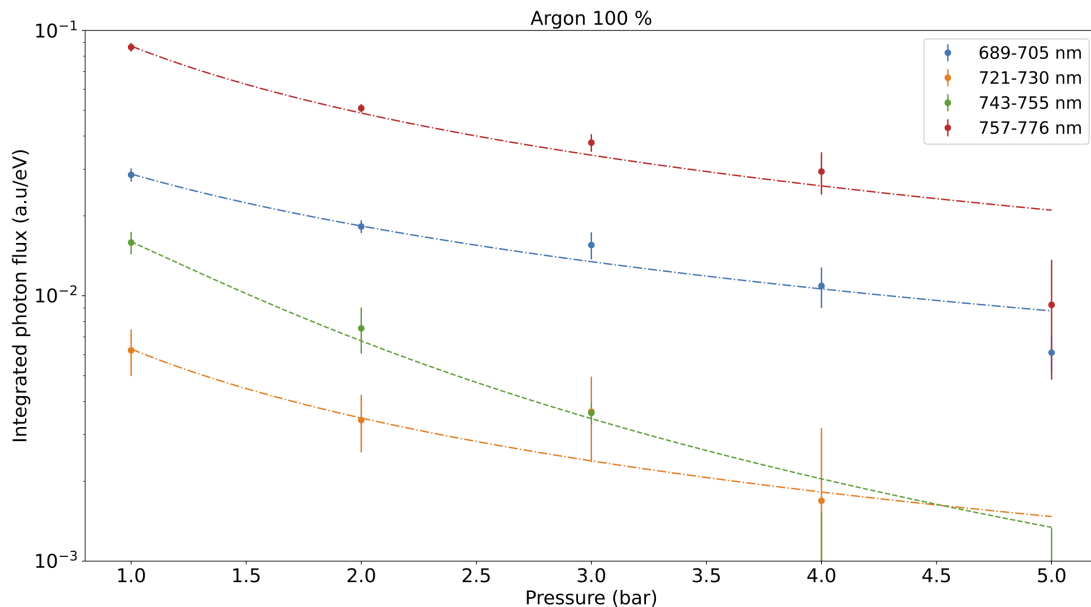


Figure 4. Integrated yields for different argon near-infrared peaks as a function of pressure. Dashed-dotted lines represent a fit to a 2-body self-quenching law while the dashed-green line follows from three-body self-quenching.

The presence of impurities can be derived from the peak at around 310 nm, corresponding to the $\text{OH}^*(A^2\Sigma^+) \rightarrow \text{OH}(X^2\Pi)$ transition [43, 44]. It can be attributed to charge transfer between Ar^+ and H_2O^+ , following dissociative recombination to populate OH^* [44]. Even if barely visible, N_2 peaks at around 335, 355 and 380 nm are present in argon too, as expected from the transfer reactions identified in [45].

3.2 Ar/ CF_4 mixtures

Figure 5 compiles the spectra for different Ar/ CF_4 admixtures and pressures. Although they were obtained at zero field, no significant dependence with the X-ray intensity or electric field was observed, demonstrating the absence of recombination effects. This was generally the case except below 1% CF_4 , conditions for which the energy of the ionization electrons is high enough to cause neutral bremsstrahlung radiation (NBrS) during their drift [46–48] at the fields required for full

charge-collection, thus complicating the interpretation. Exemplary, for the full-collection field of 2900 V/cm in pure Ar at 1 bar, NBrS would amount to about ~ 0.015 ph/eV in the region 210-800 nm [48]. Given its flat nature, NBrS easily overwhelms the 3rd continuum in the region around 200-350 nm, if assuming that the integral of the latter amounts to 0.0036 ph/eV, as recently measured in [49]. These results are not presented here as they will be discussed in detail elsewhere.

Indirectly, the low impact of recombination light in the window 210-800 nm for low CF₄ concentrations may be inferred from: i) its absence for mixtures above 1% CF₄ (e.g., Fig. 12 in appendix) for which the ionization densities are similar; ii) the fact that full charge-collection is reached to within less than 5% for all conditions (e.g., Fig. 2); iii) the fact that NBrS constitutes a featureless continuum above a certain wavelength threshold depending on the electron energy [47] and, within that assumption, no significant field-induced modification of the characteristic UV and visible bands of the Ar/CF₄ scintillation could be observed below 1% CF₄.

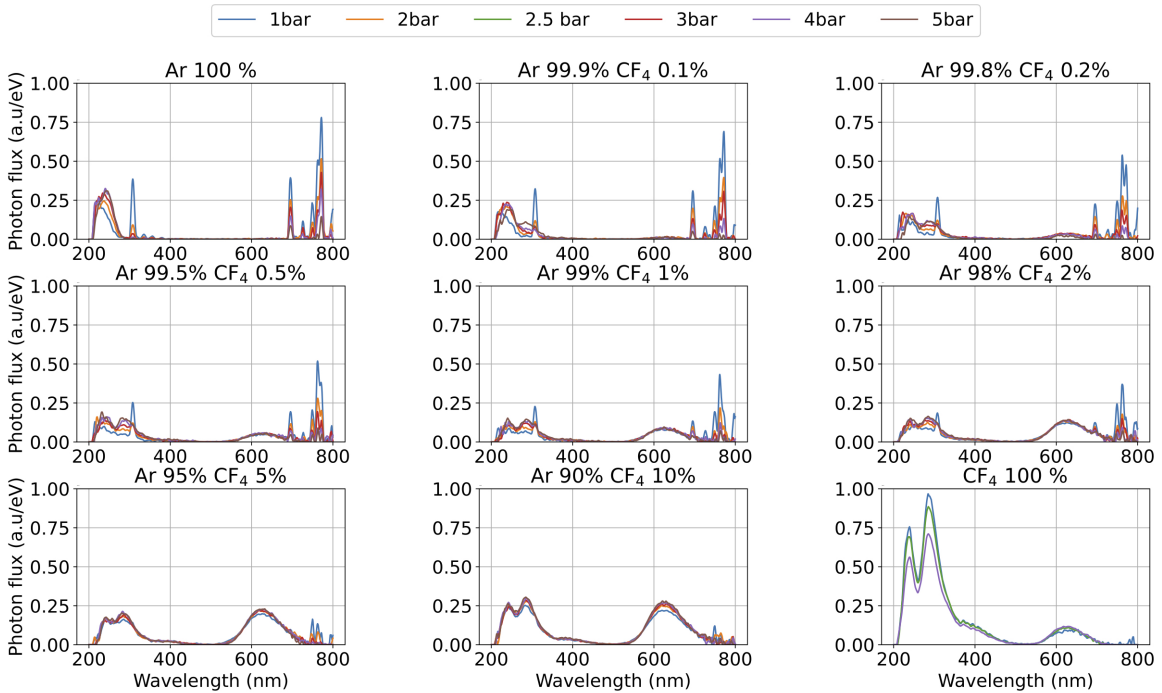


Figure 5. Emission spectra per eV of released energy for different concentrations of Ar/CF₄, at zero field. Measurements are expected to be free from recombination effects, as discussed in text. A global normalization was imposed by setting to 1 the maximum of the 290 nm peak in pure CF₄ at 1 bar. The exact CF₄ concentrations (after calibration) can be found in table 13.

In the spectra shown in Fig. 5 it can be seen that the transition between the pure-argon spectrum and the CF₄ one starts to happen as soon as 0.1% CF₄ is introduced. At that concentration, the appearance of a new peak at 290 nm and the small bump at around the CF₃^{*} band hint towards a contribution beyond that of direct CF₄ excitation, that would be otherwise suppressed 1000 times relative to the 100% CF₄ case. The 3rd continuum from argon quenches rapidly as CF₄ increases and it halves for just 0.2% CF₄. For higher concentrations, the appearance of the CF₄^{+,*} band associated to the $\tilde{C} \rightarrow \tilde{X}$ transition (centered at 230 nm) obscures the effect. As already noted, the

near-infrared emission from argon displays self-quenching as the pressure increases, but it is also strongly suppressed in the presence of CF₄, becoming undetectable above 5%CF₄ at 5 bar. The N₂ bands resulting from Ar* transfers disappear already at 0.1% CF₄, suggesting that N₂ contamination is well below that concentration, if recalling that the Ar* quenching rates are comparable for the two molecules [51]. The most prominent contamination in the system seems to be H₂O, that leads to OH* emission at around 310 nm and is arguably driven by Ar⁺ + H₂O → Ar + H₂O⁺ charge transfer [44]. Given the shape-modification observed for the UV band of CF₄ at around 1 bar (where the presence of the OH* peak is most prominent relative to higher pressures), it cannot be fully excluded that H₂O might have a small influence in that case, specially for low CF₄ concentrations. For high pressures and high CF₄ concentrations, the OH* peak vanishes and the UV spectra stabilizes. Collisional-relaxation of CF₄^{+,*}(ν) sates down to the bottom of the potential well CF₄^{+,*}(ν = 0) represents a plausible alternative, that would also explain the emergence of fully-formed UV bands when pressure and CF₄ concentration increases (as Ar is a priori inefficient for this process).

Figure 6 compiles the integrated yields in the most representative regions (210-250 nm, 250-350 nm, 350-400 nm and 400-700 nm) for different pressures and as a function of the CF₄ concentration. The trend of the 210-250 nm emission (blue) follows from the quenching of the Ar 3rd continuum, with CF₄^{+,*} emission from $\tilde{C} \rightarrow \tilde{X}$ taking over as the CF₄ concentration increases, causing a minimum for concentrations around 1% CF₄. In the other UV bands the increase is monotonous with CF₄ while the visible band shows an optimum for concentrations around or above the ones studied in this work. In general, visible-range yields are significantly increased over the ones in pure CF₄ in the range 2-10%, and can be anticipated beyond the upper concentration studied in this work. A kinetic model addressing the observed behaviour is sketched in the next section.

4 Discussion

4.1 Wavelength-shifting pathways

Our data presents strong evidence of wavelength-shifting and in particular Fig. 6 suggests, qualitatively, that scintillation in the 630 nm band (CF₃^{*}) must feed from Ar* transfers and not just through direct CF₃^{*} formation, otherwise a proportional trend would be expected. The observed increase (approximately proportional up to 1%CF₄) shows a drop above or around 10%CF₄ and might still be attributed to direct CF₃^{*} formation followed by self-quenching with CF₄. However this would imply a strong dependence with pressure, that is not seen in data. Fig. 7 shows for illustration a spectral comparison with the CF₄ and He/CF₄ systems, for which the CF₃^{*} band appears depopulated relative to the UV one, adding further support to the role of Ar* states at CF₃^{*} formation. Given that the threshold for CF₃ production sits at 12.5 eV [52] and the one for CF₃⁺ production at around 16 eV [41, 50], the threshold for CF₃^{*} production must lie in between. This indicates that the Ar* state(s) involved in transfers lie well above the lowest-lying Ar excited states at 11.5 eV and close to the continuum (IP_{Ar}=15.7 eV), thereby labeled Ar** hereafter. A discussion on the nature of such a state(s) is postponed to the end of this section. On the other hand, the UV scintillation may be tentatively attributed to transfers involving the higher-lying 3rd continuum precursors (Ar_{n=2,3}^{*,+}, Ar_{n=2,3}⁺⁺) [53]. The fact that the yields in the region 210-250 nm and 250-350 nm show opposing trends up to around 1% CF₄, with the total yield remaining approximately constant, is a good indicator that the energy is being transferred between species. The extracted quenching rates and

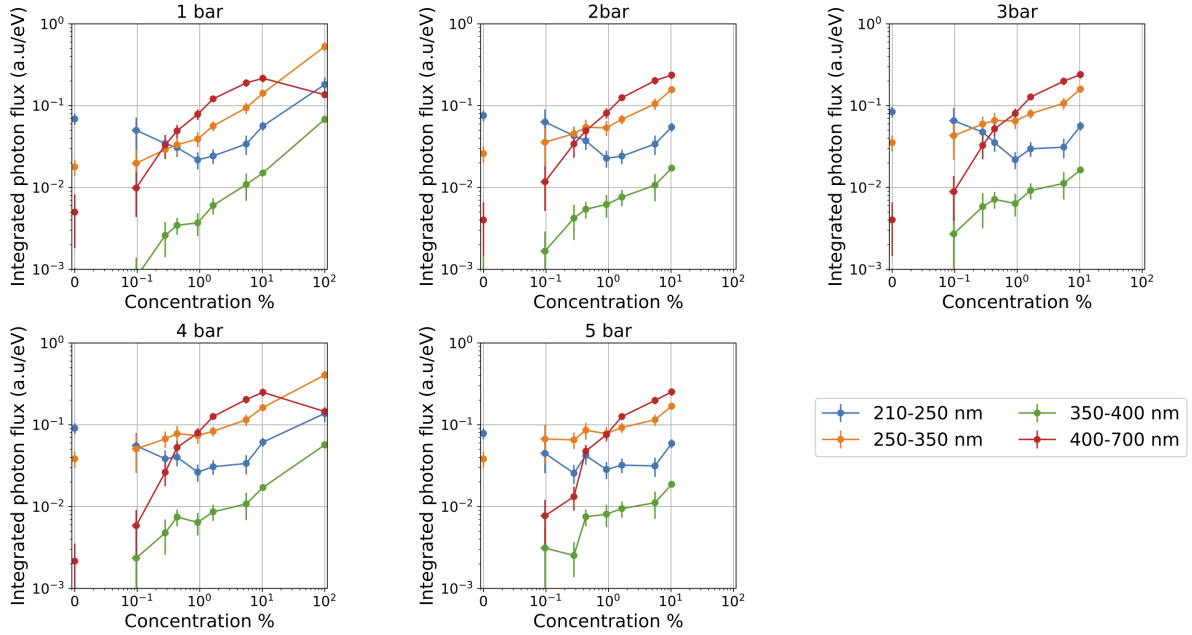
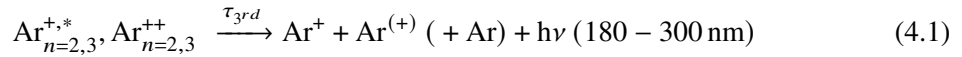


Figure 6. Integrated scintillation yields for the Ar/CF₄ system (per eV of released energy), shown in different bands as a function of CF₄ concentration, for different pressures. Zero-concentration yields have been added to the logarithmic x -axis to illustrate the asymptotic behaviour. (The argon peak located at 700 nm and the peaks caused by impurities were removed in this analysis)

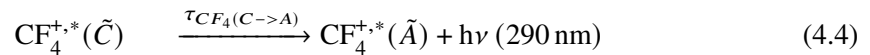
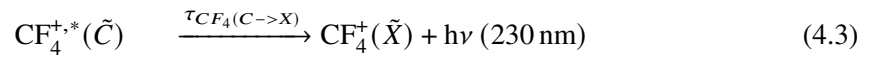
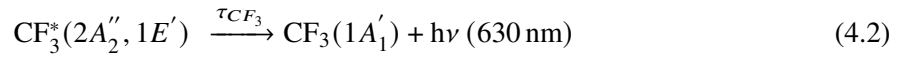
spectral shapes add further support to this interpretation, as shown later.

A kinetic model has been developed keeping the above considerations in mind, in order to quantitatively interpret our experimental results. It is sketched in Fig 8 and detailed in the following.

Aiming at a reduced number of model parameters, the 3rd continuum precursors are characterized through an effective decay constant of 5 ns (e.g., [49]):



For CF₄, the states that leave a clear footprint in the spectra can be matched to the following decays:



To the best of our knowledge, not all the possible decays of the accessible CF₄^{+,*} states have been observed in literature, e.g. CF₄^{+,*}(B) → CF₄^{+,*}(A). As CF₄^{+,*} states are unstable [41], it is possible that dissociation out-competes radiative decay in some of them. For the states involved in eqs. 4.2-4.4, however, we opted to assign a decay probability of 100% to avoid the introduction of new

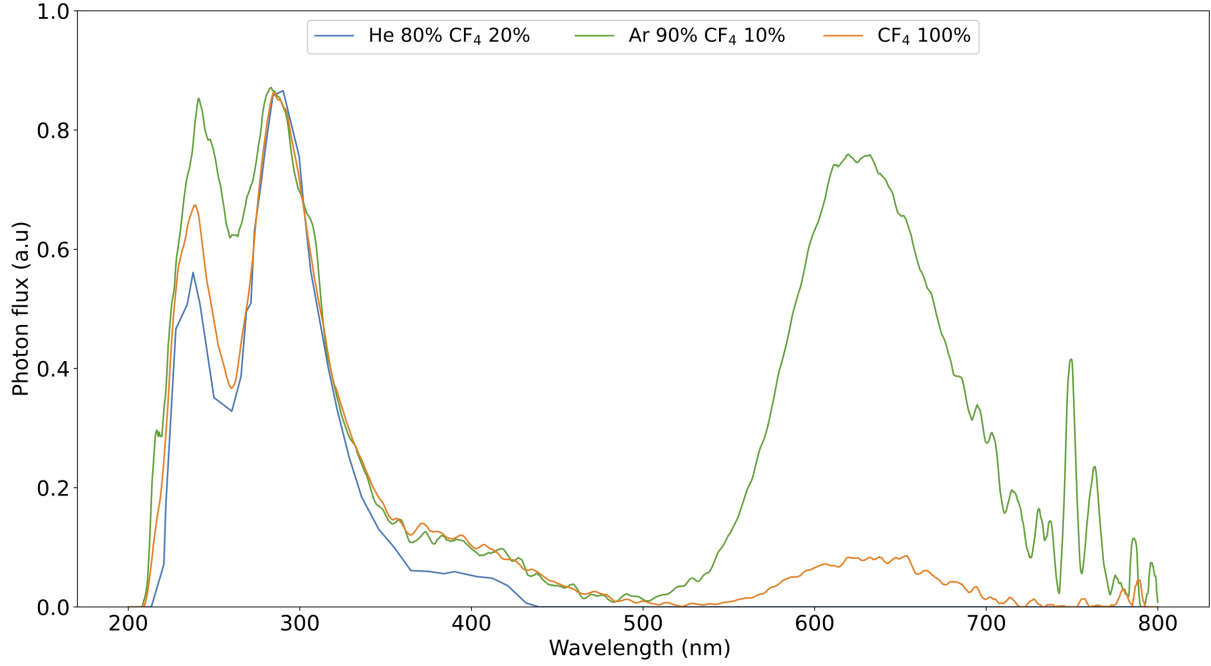
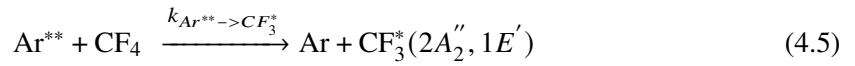


Figure 7. Comparison between the primary scintillation spectrum for pure CF_4 (orange), Ar/CF_4 at 10% per volume (green) and He/CF_4 at 20% per volume (blue), at 1 bar. All spectra have been arbitrarily normalized to the 290 nm UV peak.

additional parameters. As shown later, a good χ^2 is obtained in the proposed kinetic scheme through a global fit employing 2 parameters per spectral region (UV and visible), so a further increase in the number of parameters was deemed unnecessary.

Transfer reactions between Ar states and CF_4 represent the last ingredient. For the visible component, we make the natural assumption that transfers between the Ar^{**} state(s) and CF_4 compete just with self-quenching, summarized as:



It is in principle possible to include an additional non-radiative quenching channel of Ar^{**} with CF_4 , that has been neglected again on the basis that it is not needed to describe data and it would add unnecessary complexity to the model. Within the proposed kinetic scheme, Ar^{**} transfers would lead to CF_3^* scintillation with near-100% probability.

Last, we consider transfer reactions leading to UV emission between the 3rd continuum pre-

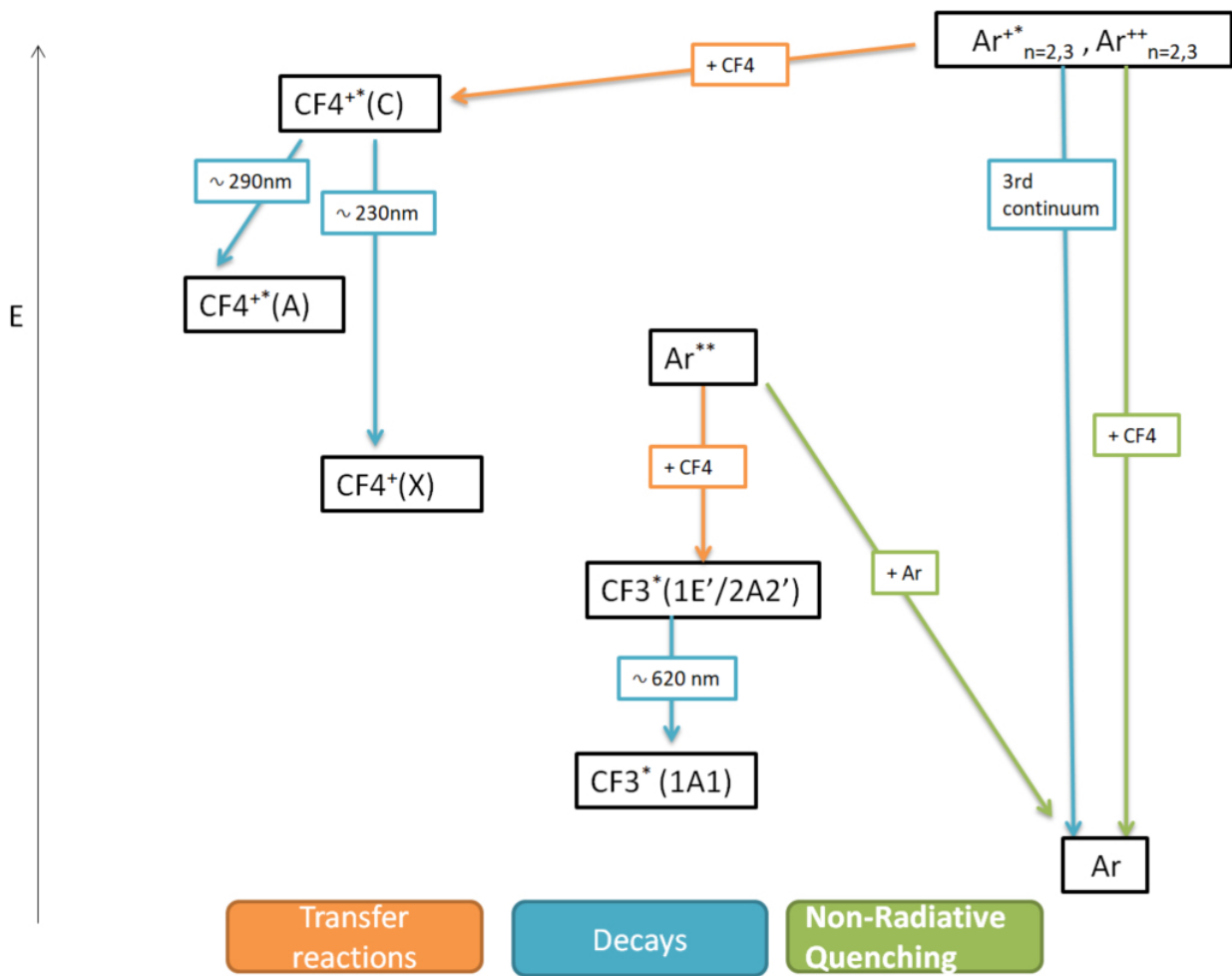
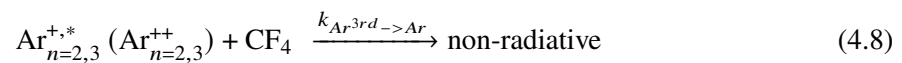
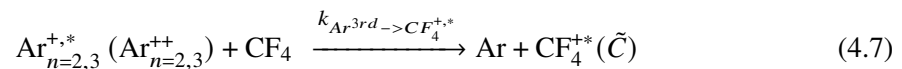


Figure 8. Kinetic scheme used to describe wavelength-shifting in Ar/CF₄ mixtures. The main scintillation drivers are the CF₄^{+,*}, CF₃^{*} and Ar 3rd continuum states. Energy considerations lead to the hypothesis of an additional high-lying Ar^{**} state, whose nature is discussed in text.

cursors and CF₄, together with a quenching reaction to non-radiative states:



where rates for transfer and non-radiative quenching have been introduced for an ‘effective’ 3rd continuum precursor. Along this line, reactions of 3rd continuum states with ground-state Ar are assumed to be already accounted for when considering the kinetics of such an ‘effective’ precursor, and remain unaltered in the presence of CF₄ (for a detailed pathway scheme of the 3rd continuum formation, the reader is referred to [53]). In the following, reaction rates [*t*⁻¹] are defined for 1 bar of the reactive, and scaled based on pressure and species concentration (as done for instance in [27]).

Before evaluating the model, it should be noted that the possibility of self-quenching of the $CF_3^*(2A_2'', 1E')$ state with CF_4 has been omitted due to the negligible pressure-dependence of Ar/ CF_4 scintillation in the 630 nm band. $CF_4^{+,*}$ states, on the other hand, evidence a small self-quenching on the UV region in pure CF_4 , compounded with the aforementioned indications of collisional relaxation for Ar/ CF_4 mixtures at low pressures and CF_4 concentrations. Such dependences with pressure can be easily included in the model but, being a small effect and not shedding light into the main transfer mechanisms, they have been omitted for the sake of simplicity. The near-visible band centered around 364 nm, arising from the $\tilde{D} \rightarrow \tilde{C}$ transition, is also not considered given its relatively small contribution to the total spectrum.

From the above set of reactions, it is possible to derive the scintillation probability (per eV of energy deposited in the medium) of the states $CF_3(2A_2'', 1E')$, $CF_4^{+,*}(\tilde{C})$, and of the effective state Ar^{3rd} :

$$P_{\gamma,CF_3^*} = f_{CF_4} \cdot P_{\gamma,CF_3^*}|_{dir} + \left((1 - f_{CF_4}) \cdot P_{Ar^{**}} \cdot \frac{K_{Ar^{**} \rightarrow CF_3^*}}{K_{Ar^{**} \rightarrow CF_3^*} + \frac{(1-f_{CF_4})}{f_{CF_4}} \cdot K_{Ar^{**} \rightarrow Ar^{**}}} \right) \quad (4.9)$$

$$P_{\gamma,CF_4^{+,*}} = f_{CF_4} \cdot P_{\gamma,CF_4^{+,*}}|_{dir} + \left((1-f_{CF_4}) \cdot P_{Ar^{3rd}} \cdot \frac{f_{CF_4} \cdot n \cdot K_{Ar^{3rd} \rightarrow CF_4^{+,*}}}{1/\tau_{3rd} + f_{CF_4} \cdot n \cdot (K_{Ar^{3rd} \rightarrow CF_4^{+,*}} + K_{Ar^{3rd} \rightarrow Ar})} \right) \quad (4.10)$$

$$P_{\gamma,Ar^{3rd}} = (1 - f_{CF_4}) \cdot P_{Ar^{3rd}} \cdot \left(\frac{1/\tau_{3rd}}{1/\tau_{3rd} + f_{CF_4} \cdot n \cdot (K_{Ar^{3rd} \rightarrow CF_4^{+,*}} + K_{Ar^{3rd} \rightarrow Ar})} \right) \quad (4.11)$$

Here f_{CF_4} represents the CF_4 concentration, n equals the pressure ratio P/P_0 , and the quenching and transfer rates are the ones defined in 4.5-4.8. Parameters with subscript 'dir' refer to the probability of direct scintillation, and $P_{Ar^{**}}$, $P_{Ar^{3rd}}$ stand for the formation probability of the Ar^{**} state(s) and of the 3rd continuum precursors, respectively. Some of the parameters needed to evaluate the above equations can be constrained based on existing experimental data, including this work. The direct scintillation probabilities, for instance, as well as the probability of formation of 3rd continuum precursors, can be obtained from the yields in pure CF_4 and pure argon. The time constant for the argon 3rd continuum has been taken from [49]. Further, based on the model structure, only the ratio of Ar^{**} transfer to quenching rates in 4.9 is relevant, reducing the total number of fit parameters to four. The other three parameters represent the formation probability of Ar^{**} states, and the non-radiative quenching and transfer rates of $CF_4^{+,*}$. The model structure also makes explicit the lack of pressure-dependence of CF_3^* scintillation observed for any admixture.

A weighted global fit of the proposed kinetic model to the three data series associated with the 230, 290 and 630 nm bands was performed. Yields in the first two bands were fitted to a sum of eqs. 4.10 and 4.11 and the 630 nm band was described through eq. 4.9. The fit is shown in Fig 9 for a pressure of 4 bar (blue, orange, red lines), alongside the corresponding experimental data (full circles). Its reduced χ^2 of 1.56 adds plausibility to the present interpretation. The

following values and uncertainties were obtained for the fit parameters: $P_{Ar^{**}}/P_{Ar^{3rd}} = 3.19 \pm 0.39$ (population of Ar^{**} relative to that of 3^{rd} continuum precursors); $\frac{K_{Ar^{**} \rightarrow CF_3^+}}{K_{Ar^{**} \rightarrow Ar^*}} = 36.5 \pm 7.9$ (ratio of transfer to collisional quenching of Ar^{**}); $K_{Ar^{3rd} \rightarrow CF_4^{+,*}} = 49 \pm 18 \text{ ns}^{-1}$ (transfer rate of the Ar^{3rd} continuum) and $K_{Ar^{3rd} \rightarrow Ar} = 4.1 \pm 3.3 \text{ ns}^{-1}$ (non-radiative quenching of the Ar^{3rd} continuum). Within the proposed kinetic model, the ratio of transfer-mediated scintillation to direct scintillation can be computed: for 1% CF_4 , illustratively, values as large as 72 ± 20 (visible) and 20.9 ± 2.1 (UV) are obtained.

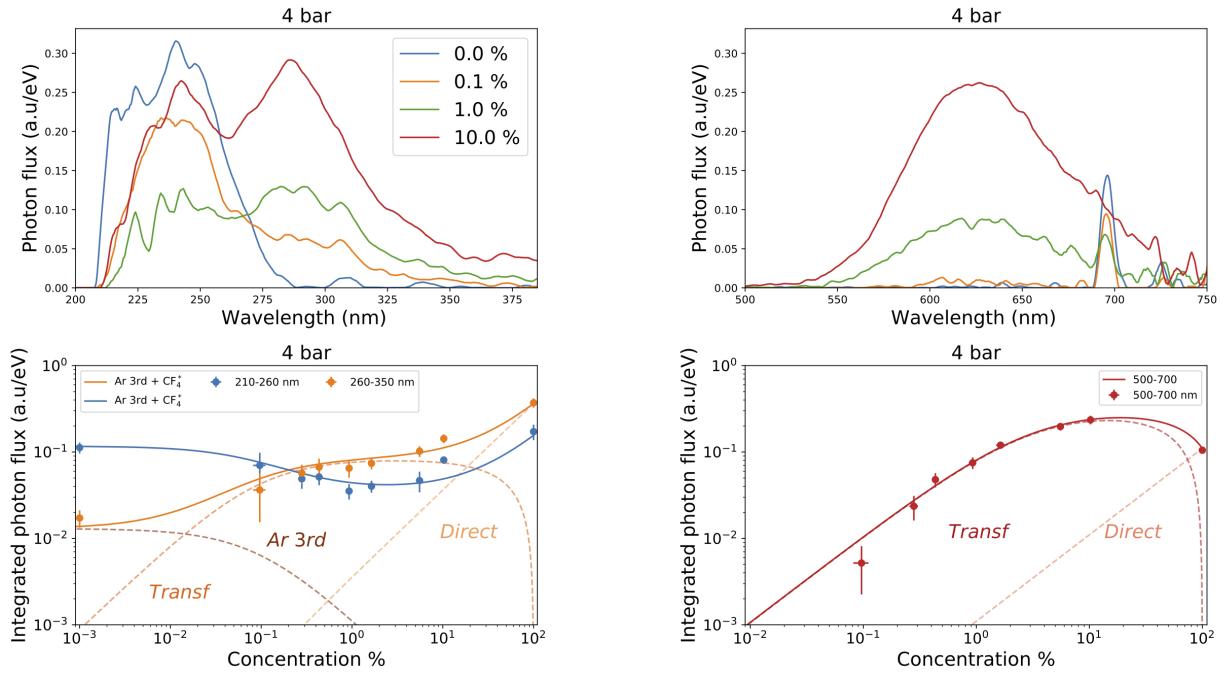


Figure 9. Top row: scintillation spectra for different CF_4 concentrations at 4 bar, zoomed in the ultraviolet (left) and visible (right) regions. Bottom row: integrated yields on the ultraviolet (left) and visible (right) regions (shown as closed circles), superimposed to the kinetic model introduced in text. The experimental value for zero concentration is added on the bottom-left plot at 0.001% CF_4 , taking advantage of the fact that the model asymptotically tends to a constant in that case.

In the UV-band, a detailed analysis of the spectral shapes (Fig. 9 top-left) brings additional support to the proposed interpretation: as soon as 0.1% CF_4 is added to argon, there is a strong suppression of the argon 3^{rd} continuum, coinciding with the appearance of the 290 nm peak from $CF_4^{+,*}$. For 1% CF_4 , the effect is even more clear. Taking as a reference the yields measured earlier for α -particles in the Ar^{3rd} continuum (around 3500 ph/MeV [49]) and in the VUV-visible range of CF_4 (1000-3000 ph/MeV [3, 5, 10, 11]), it is implausible that direct CF_4 excitation could be responsible for the observed levels of X-ray scintillation when the species is present at a mere sub-percent level. Above 1% CF_4 , the overlap between argon 3^{rd} continuum and the $CF_4^{+,*}$ emission at 230 nm complicates a qualitative description, and a direct comparison with the proposed kinetic

model has to be used instead (Fig. 9 bottom-left). In any case, the fact that the number of photons emitted in the UV region is maintained approximately constant when transfer reactions dominate (i.e., below a few % CF₄) reinforces the idea that the kinetics of the Ar 3rd continuum states drives the UV scintillation of the admixture, and that the CF₄^{+,*} state scintillates efficiently upon transfer, as assumed. Although the agreement seems convincing, additional support to the proposed pathway scheme can be found: according to the model, the scintillation of the argon 3rd continuum gets quenched down to just 8.6% ± 2.8% of its nominal value in the pure gas when in presence of 1% CF₄. This is compatible with the quenching level that has been reported for the Ar 3rd continuum when admixed with CO₂, at about 1% concentration [54]. Given that both CF₄ and CO₂ are energetically accessible to transfers from the high-lying Ar_{2,3}^{+,*} and Ar_{2,3}⁺⁺ states, and the similar molecule size, this approximate agreement is reassuring.

In the visible band, the proposed model where CF₃^{*} formation competes with self-quenching provides a natural explanation for the total absence of pressure dependencies. It requires, however, the somewhat artificial introduction of a new Ar^{**} state or set of states. Invoking the 3rd continuum precursors cannot be excluded, although it would require increasing the model complexity substantially: the behaviour of the transfer reactions involved in UV and visible scintillation (Fig. 9-bottom) is too different to be easily attributable to the same state. As discussed earlier, the existence of Ar^{**} states is justified by energy considerations, given that they must be several eV above the Ar^{*} 2nd continuum precursors at around 11.5 eV, yet below the argon IP (15.7 eV) in order to induce excited dissociation of CF₃^{*}. According to our model, the formation probability of Ar^{**} is about ×3 that of Ar^{3rd} states, that would imply (if using for reference the 2nd and 3rd continuum yields measured in [49]) a substantial part of the available Ar excited states being eligible for transfer (about 50%). Also, the transfer rate would need to be nearly 40 times larger than self-quenching with Ar (36.5 ± 7.9 from our fit) and it remains open which mechanism could cause such large transfer values. Although the role of the Ar^{**} states cannot be excluded from present results, there is an alternative explanation in the formation of an ArCF₃^{*} exciplex. There is apparently no information in literature about this process that is, e.g., generally absent in the modelling of Ar/CF₄ discharges [55–57]. ArCF₃ is iso-electronic with CF₄⁻ that is in fact known not to be stable, except for (CF₄)_n clusters [58]. There are suggestions of the formation of the (expectedly more stable) CF₄^{-,*} state in some works (e.g. [59]), but not enough evidence is provided. If the binding energy of such an exciplex would be on the order of few eV, it is conceivable that it could be formed starting from the long-lived Ar₂^{*} triplet state. Although speculative at the moment, such a mechanism would provide a natural explanation for the lack of pressure-dependence, the similarity between the populations of Ar^{**} and 2nd continuum precursors, as well as for the preponderance of wls-transfers in Ar compared to, e.g., He.

4.2 Comparison with previous results

The results obtained in this work may be compared with the ones obtained for Ar/CF₄ mixtures in a 9 MeV proton beam at 1 bar in [60]. Little details are found there in regard to space charge, recombination and beam-induced scintillation and in fact the relative normalization of the visible/UV bands is not given either. Qualitatively, it is possible to see that the relative increase in both the visible and UV bands from 1% to 10% CF₄ concentrations is around a factor 3, compatible with present results. The region above 700 nm is characterized by the presence of an additional

molecular emission while the Ar IR emission appears fully quenched, both observations being in stark contrast with our results. The absence of data for pure CF₄ together with the strong contamination found for argon data in that work, preclude any estimate of the photon yields or wavelength-shifting capability.

A spectral comparison between scintillation induced by X-rays (this work) and α -particles (in [3]) seems more reliable at this point, and can be seen in Fig. 3 (orange, dashed). Both spectra were obtained at 1 bar, arbitrarily normalized to the 290 nm peak. They display an approximate agreement in the UV and blue regions, however the emission in the red region appears off by a factor of 2.8. The discrepancy is preserved when considering the ratio between the other two UV peaks and the CF₃^{*}(2A₂'', 1E') \rightarrow CF₃(1A₁') one at 630 nm. These transitions are well above the calibration mark of the lamp at 300 nm and also far enough into the visible region so that we can safely exclude any strong wavelength-asymmetry of the light collection process in the chamber compared to the calibration setup. As no hints of charge recombination were observed at 1 bar neither in [3] nor in this work, these measurements point to a fundamental difference between the scintillation mechanisms for α particles and X-rays in CF₄.

Last, it must be recalled that the strength of CF₄ scintillation in the VUV-visible range, as obtained for α particles at 1 bar, is currently found at levels of 1000-3000 ph/MeV [3, 5, 10, 11]. Values within this range have been reported, too, for Ar/CF₄ mixtures around 10 bar in [23]. Nonetheless, the large experimental spread on the above CF₄ yields, together with the particle-dependence of the spectral emission reported here, call for future studies on the scintillation yields of these type of mixtures.

5 Conclusions

We have presented a comprehensive data-set on the primary scintillation spectra of Ar/CF₄ mixtures in the pressure range 1-5 bar and CF₄ concentrations from 0.1 to 10%, including pure gases. Our results, obtained under strong X-ray irradiation yet in conditions shown to be free from recombination and space charge effects, provide a clear indication that Ar 3rd-continuum precursors play a pivotal role in the UV-scintillation of Ar/CF₄ mixtures. On the other hand, a high-lying Ar^{**} state or an ArCF₃^{*} exciplex seem the most plausible candidates leading to CF₃^{*} formation (responsible for the scintillation in the visible range), with a simple pathway scheme explaining the observed phenomenology, in particular the lack of pressure-dependence of the measured yields. The proposed kinetic model resorts to just 4 parameters (2 per emission band), achieving a satisfactory agreement with a reduced χ^2 of 1.56. A more complex mechanism starting from the precursors of the Ar 3rd continuum could still be advocated to cause scintillation in the visible range, however its elucidation does not seem accessible to present experimental conditions.

In sum, wavelength-shifting in the Ar/CF₄ system is very strong for the conditions studied: at a mere 2% CF₄, for instance, scintillation in the 500-700 nm (CF₃^{*}) band exceeds that of pure CF₄ with independence from pressure. UV scintillation remains at strengths comparable to the visible one in the concentration range 1-10% CF₄, and progressively dominates outside it. Overall, upon just 1% CF₄ addition, the ratio of transfer-mediated scintillation to direct scintillation is estimated to be as large as 72 ± 20 (visible) and 20.9 ± 2.1 (UV).

Our measurements convey as well strong evidence of the dependence of the spectra of emission on particle type. The ratio of the UV/visible bands, as observed for X-rays in this work, is about $\times 2.8$

larger than measured earlier for α 's in pure CF₄ at around 1 bar, both performed in recombination-free conditions. Overall, the presented results show great promise for technological applications in future particle detectors in the fields of rare event searches, nuclear and neutrino physics.

Acknowledgements

The authors want to thank Saulo Vázquez (USC) for his valuable insights on the chemistry of Ar/CF₄ reactions and L. Margato (LIP-Coimbra) for useful feedback. This research was funded by the Spanish Ministry ('Proyectos de Generación de Conocimiento', PID2021-125028OB-C21), Xunta de Galicia (Centro singular de investigación de Galicia, accreditation 2019-2022), and by the "María de Maeztu" Units of Excellence program MDM2016-0692. DGD was supported by the Ramón y Cajal program (Spain) under contract number RYC-2015-18820.

References

- [1] D. Nygren, *The Time Projection Chamber - A new 4 π detector for charged particles*, PEP-144-1974.
- [2] D. González-Díaz, F. Monrabal, S. Murphy, Gaseous and dual-phase time projection chambers for imaging rare processes, *Nuclear Instruments and Methods in Physics Research Section A: Accelerators, Spectrometers, Detectors and Associated Equipment* **878** (2018) 200.
- [3] A. Morozov et al., Photon yield for ultraviolet and visible emission from CF₄ excited with alpha particles, *Nuclear Instruments and Methods in Physics Research, Section B: Beam Interactions with Materials and Atoms* **268(9)** (2010) 1456–1459.
- [4] A. Morozov et al., Effect of the electric field on the primary scintillation from CF₄, *Nuclear Instruments and Methods in Physics Research Section A: Accelerators, Spectrometers, Detectors and Associated Equipment* **628(1)** (2011) 360-363.
- [5] A. Pansky, A. Breskin, A. Buzulutskov, R. Chechik, V. Elkind, and J. Va'vra, The scintillation of CF₄ and its relevance to detection science, *Nuclear Inst. and Methods in Physics Research A* **354(2-3)** (1995), 262–269.
- [6] M. M. F. R. Fraga, F. A. F. Fraga, S. T. G. Fetal, L. M. S. Margato, R. F. Marques, and A. J. P. L. Policarpo., The GEM scintillation in He–CF₄, Ar–CF₄, Ar–TEA and Xe–TEA mixtures, *Nuclear Instruments and Methods in Physics Research Section A: Accelerators, Spectrometers, Detectors and Associated Equipment* **504(1-3)** (2003) 88–92.
- [7] A. Morozov, L. M. S. Margato, M. M. F. R. Fraga, L. Pereira, and F. A. F. Fraga., Secondary scintillation in CF₄: Emission spectra and photon yields for MSGC and GEM., *Journal of Instrumentation* **7(2)** (2012).
- [8] D. González-Díaz, A survey on GEM-based readouts and gas mixtures for optical TPCs, Vienna Conference 2016, <https://indico.cern.ch/event/391665/contributions/1827205/>.
- [9] L. G. Christophorou and J. K. Olthoff. *Fundamental Electron Interactions with Plasma Processing Gases*, Kluwer Academic/Plenum Publishers, New York, NY, 2004.
- [10] B. Azmoun et al., A measurement of the scintillation light yield in CF(4) using a photosensitive GEM detector., *IEEE Trans. Nucl. Sci.* **57** (2010) 2376–2381.
- [11] G. Lehaut, S. Salvador, J. M. Fontbonne, F. R. Lecolley, J. Perronnel, and C. Vandamme, Scintillation properties of N₂ and CF₄ and performances of a scintillating ionization chamber., *Nuclear Instruments and Methods in Physics Research, Section A: Accelerators, Spectrometers, Detectors and Associated Equipment* **797** (2015) 57–63.

- [12] J. B. R. Battat et al., The Dark Matter Time Projection Chamber 4Shooter directional dark matter detector: Calibration in a surface laboratory., *Nuclear Instruments and Methods in Physics Research, Section A: Accelerators, Spectrometers, Detectors and Associated Equipment* **755** (2014), 6–19.
- [13] M. Takahashi et al., Development of an Electron-Tracking Compton Camera using CF₄ gas at high pressure for improved detection efficiency., *Nuclear Instruments and Methods in Physics Research, Section A: Accelerators, Spectrometers, Detectors and Associated Equipment* **628(1)** (2011) 150–153.
- [14] H. M. Araújo et al., The MIGDAL experiment: Measuring a rare atomic process to aid the search for dark matter., *Astroparticle Physics* **151** (2022) 102853.
- [15] E. Baracchini et al., Stability and detection performance of a GEM-based Optical Readout TPC with He/CF₄ gas mixtures., *Journal of Instrumentation* **15(10)** (2020) P10001.
- [16] M. M. R. Fraga, C. C. Bueno, J. A. C. Gonçalves, F. A. F. Fraga, R. Ferreira Marques, and A. J. P. L. Policarpo, Pressure dependence of secondary NIR scintillation in Ar and Ar/CF₄., *IEEE Transactions on Nuclear Science* **48(3 I)** (2001) 330–335.
- [17] F. A. F. Fraga et al., CCD readout of GEM-based neutron detectors., *Nucl. Instrum. Meth. A* **478** (2002) 357–361.
- [18] F. M. Brunbauer et al., Live event reconstruction in an optically read out GEM-based TPC., *Nuclear Instruments and Methods in Physics Research, Section A: Accelerators, Spectrometers, Detectors and Associated Equipment* **886** (2018) 24–29.
- [19] M. Pomorski et al., Proton spectroscopy of Ni 48, Fe 46, and Cr 44., *Phys. Rev. C - Nucl. Phys* **90** (2014) 1–12.
- [20] W. R. Zimmerman., Direct observation of the second 2+ state in ¹²C., *PhD Thesis*
<https://opencommons.uconn.edu/dissertations/230/>
- [21] B. Abi et al (DUNE Collaboration) , Volume I. Introduction to DUNE. , *JINST* **15(2020)**T08008.
- [22] A. Abed Abud, et al., (DUNE Collaboration), A Gaseous Argon-Based Near Detector to Enhance the Physics Capabilities of DUNE arXiv:2203.06281v1.
- [23] P. Amedo et al., Primary scintillation yields of α particles in pressurized Argon-CF₄ mixtures, in preparation. Preliminary results in LIDINE 2021, <https://indico.physics.ucsd.edu/event/1/contributions/62/>.
- [24] A. Saá-Hernández et al, On the determination of the interaction time of GeV-neutrinos in large argon-gas TPCs, on preparation for submission to JHEP.
- [25] A. Abed Abud, et al. (DUNE Collaboration)., Deep Underground Neutrino Experiment (DUNE) Near Detector Conceptual Design Report, *Instruments*, **5(4)** (2021) 31.
- [26] ICRU (report 90), Key Data for Ionizing-Radiation Dosimetry: Measurement Standards and Applications, Volume 14, Issue 1, April 2014.
- [27] C. D. R. Azevedo et al., Microscopic simulation of xenon-based optical TPCs in the presence of molecular additives., *Nuclear Instruments and Methods in Physics Research, Section A: Accelerators, Spectrometers, Detectors and Associated Equipment* **877** (2018) 157–172.
- [28] M.J. Berger et al., XCOM: Photon Cross Section Database (version 1.5). (2010) [Online] Available: <http://physics.nist.gov/xcom> [2023, April 17]. National Institute of Standards and Technology, Gaithersburg, MD.
- [29] C. D. R. Azevedo et al., Pressure effects on the X-ray intrinsic position resolution in noble gases and mixtures., *Journal of Instrumentation*, **11(12)** (2016) P12008–P12008.

- [30] B. Al Atoum, S. F. Biagi, D. González-Díaz, B. J. P. Jones, and A. D. McDonald., Electron Transport in Gaseous Detectors with a Python-based Monte Carlo Simulation Code, *Comput. Phys. Commun.* **254** (2020) 107357.
- [31] Sandro Palestini and Kirk T. McDonald, Space Charge in Ionization Detectors, <http://kirkmcd.princeton.edu/examples/spacecharge.pdf>
- [32] COMSOL Multiphysics® www.comsol.com. COMSOL AB, Stockholm, Sweden.
- [33] L. M. S. Margato, A. Morozov, L. Pereira, M. M. F. R. Fraga, and F. A. F. Fraga., Effect of the gas contamination on CF 4 primary and secondary scintillation, *Nucl. Instr. Meth. A* **695**(2012) 425.
- [34] G. F. Reinking, L. G. Christophorou, and S. R. Hunter., Studies of total ionization in gases/mixtures of interest to pulsed power applications, *Journal of Applied Physics* **60**(2) (1986) 499–508.
- [35] E. Robert, A. Khacef, C. Cachoncille, J.M. Pouvesle., Time-resolved spectroscopy of high pressure rare gases excited by an energetic flash X-ray source, *Optics Communications* **117** (1995) 179-188.
- [36] N. Washida, M. Suto, S. Nagase, U. Nagashima, and K. Morokuma., Emission spectra of CF3 radicals. IV. Excitation spectra, quantum yields, and potential energy surfaces of the CF3 fluorescences., *The Journal of Chemical Physics* **78**(3) (1983) 1025–1032 .
- [37] L. C. Lee, X. Wang, and M. Suto., Fluorescence from extreme ultraviolet photoexcitation of CF4, *The Journal of Chemical Physics* **85**(11) (1986) 6294–6300
- [38] M. Suto, N. Washida, H. Akimoto, and M. Nakamura., Emission spectra of CF 3 radicals. III. Spectra and quenching of CF 3 emission bands produced in the VUV photolyses of CF 3 Cl and CF 3 Br, *The Journal of Chemical Physics* **78**(3) (1983).
- [39] I. R. Lambert, S. M. Mason, R. P. Tuckett, and A. Hopkirk., Decay pathways of excited electronic states of Group IV tetrafluoro and tetrachloro molecular ions studied with synchrotron radiation, *The Journal of Chemical Physics* **89**(5) (1988).
- [40] W. R. Harshbarger, M. B. Robin, and E. N. Lassette., The electron impact spectra of the fluoromethanes, *Journal of Electron Spectroscopy and Related Phenomena* **1**(4) (1972).
- [41] W. Zhang, G. Cooper, T. Ibuki, and C. E. Brion., Excitation and ionization of freon molecules. I. Absolute oscillator strengths for the photoabsorption (12–740 eV) and the ionic photofragmentation (15–80 eV) of CF4., *Chemical Physics* **137**(1–3) (1989).
- [42] J. Reader, C. H. Corliss, W. L. Wiese, and G. A. Martin., Natl. Stand. Ref. Data Ser., Natl. Bur. Stand. (U.S.) **68** (1980).
- [43] U. Müller, Th. Bubel, G. Schulz., Electron impact dissociation of H₃O: emission cross sections for OH*, OH**, H* and H₂*O, *Z Phys D - Atoms, Molecules and Clusters* **25** (1993) 167–174.
- [44] A. Maslaáni and V. Sember, Emission spectroscopy of OH radical in Water-Argon Arc Plasma Jet, *J. of Spectroscopy* **952138** (2014).
- [45] T. Takahashi, S. Himi, M. Suzuki, J. Ruan(Gen), and S. Kubota., Emission spectra from Ar-Xe, Ar-Kr, Ar-N₂, Ar-CH₄, Ar-CO₂ and Xe-N₂ gas scintillation proportional counters, *Nuclear Instruments and Methods in Physics Research* **205** (1983) 591-596
- [46] A. Buzulutskov et al., *Revealing neutral bremsstrahlung in two-phase argon electroluminescence*, *Astropart. Phys.* **103** (2018) 29.
- [47] C. A. O. Henriques, P. Amedo et al., Neutral Bremsstrahlung emission in xenon unveiled, *Physical Review Letters X* **12**(2) (2022) 21005.

- [48] P. Amedo, D. González-Díaz and B.J.P. Jones, Neutral bremsstrahlung in TPCs, *Journal of Instrumentation* **17** (2022).
- [49] R. Santorelli et al., Spectroscopic analysis of the gaseous argon scintillation with a wavelength sensitive particle detector, *The European Physical Journal C* (2021) 81:622.
- [50] L. G. Christophorou, J. K. Olthoff, and M. V. V. S. Rao., Electron Interactions with CF₄, *Journal of Physical and Chemical Reference Data* **25(5)**, (1996), 1341–1388.
- [51] J. E. Velazco, J. H. Kolts, and D. W. Setser., Rate constants and quenching mechanisms for the metastable states of argon, krypton, and xenon., *The Journal of Chemical Physics*, **69(10)**, (1978) 4357–4373.
- [52] H. F. Winters and M. Inokuti, Total dissociation cross section of CF₄ and other fluoroalkanes for electron impact, *Phys. Rev. A* **3** (1982) 1420–1430.
- [53] J. Wieser, A. Ulrich, A. Fedenev and M. Salvermoser. , Novel pathways to the assignment of the third rare gas excimer continua, *Optics Communications* **173** (2000) 233-245.
- [54] T. D. Strickler and E. T. Arakawa. Optical emission from argon excited by alpha particles: Quenching studies. *The Journal of Chemical Physics*, **41(6)** (1964) 1783–1789.
- [55] Zhen-Hua Bi et al., Numerical results for the Ar and CF₄ mixture gas in a dual frequency capacitively coupled plasma using a hybrid model, *Physics of Plasmas*, **16** (2009) 043510.
- [56] Chenjie Bai et al., Effects of CF₄ content on particle densities and reaction pathways in atmospheric-pressure Ar/CF₄ pulsed dielectric barrier discharge plasma, *Journal of Physics D: Applied Physics*, **51** (2018) 255201.
- [57] D. A. Toneli et al., A global model study of low pressure high density CF₄ discharge, *Plasma Sources Sci. Technol.* **28** (2019) 025007.
- [58] G. L. Gutsev, L. Adamowicz The structure of the CF₄⁻ anion and the electron affinity of the CF₄ molecule, *The Journal of Chemical Physics* **102** (1995) 9309.
- [59] S.V.K. Kumar et al., Anion formation by electron impact from CF₄, *International Journal of Mass Spectrometry*, **277** (2008) 57–61.
- [60] J. Liu et al., Primary scintillation characteristics of Ar+CF₄ gas mixtures excited by proton and alpha particles. *Nuclear Instruments and Methods in Physics Research Section A: Accelerators, Spectrometers, Detectors and Associated Equipment*, **694** (2012) 157–161.
- [61] B. Walter, W. Riefler and L. Roland., Particle Detection with Drift Chambers, Springer Berlin, Heidelberg, 2008
- [62] M. A. G. Santos et al., Experimental ion mobility measurements for the LCTPC collaboration—Ar-CF₄ mixtures, *Journal of Instrumentation* **13** (2018) P04012.
- [63] L. Onsager., Initial recombination of ions ,*Phys. Rev.* **54** (1938) 554.
- [64] G. Jaffé., Zur Theorie der Ionisation in Kolonnen, *Ann. Phys.* **42** (1912) 303.
- [65] M. Boutillon., Volume recombination parameter in ionization chambers, *Phys. Med. Biol.* **43(8)** (1998) 2061-72.
- [66] T. R. Connor, M. Biondi., Dissociative Recombination in Neon: Spectral Line-Shape Studies, *Phys. Rev.* **140** (1965)A778. (Ask Diego)
- [67] L. Frommhold, M. A. Biondi., Interferometric Study of Dissociative Recombination Radiation in Neon and Argon Afterglows, *Phys. Rev.* **185** (1969) 244.

[68] J. F. Ziegler, M. D. Ziegler, and J. P. Biersack., SRIM - The stopping and range of ions in matter., *Nuclear Instruments and Methods in Physics Research, Section B: Beam Interactions with Materials and Atoms* **268(11–12)** (2010) 1818–1823.

A Electric field in the ionization volume

An axisymmetric finite-element simulation of the electrified cell and the vessel walls was performed with COMSOL Multiphysics® [32]. As shown in Fig. 10-bottom, the electric field is uniform over a region slightly exceeding 2 cm, considerably larger than the size of the ionization volume (collimated down to 1 cm at the chamber entrance -green dashed lines). The values of the electrical potential in 3D, together with the equipotential curves, are shown in Fig. 10-top.

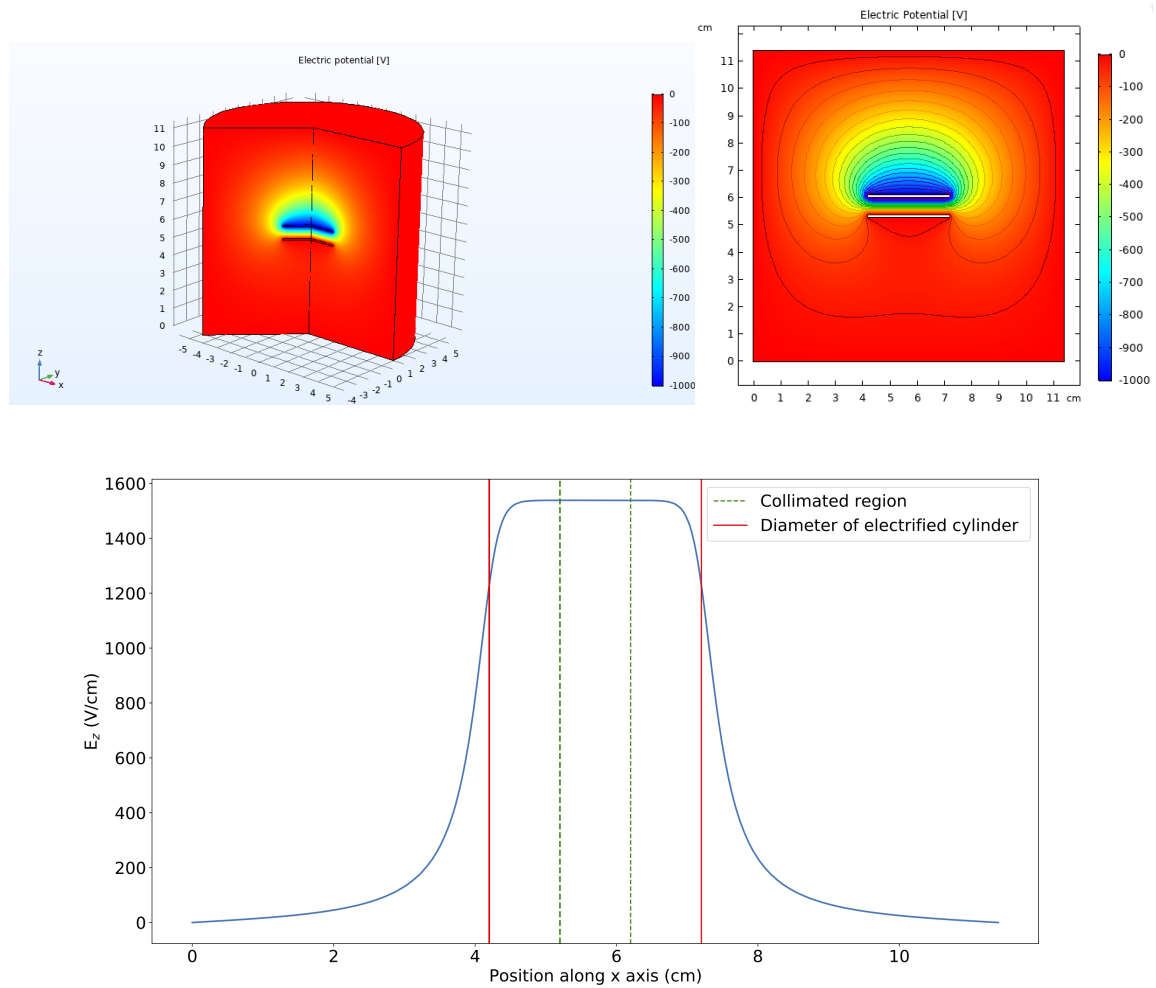


Figure 10. Results from an axisymmetric COMSOL simulation, with the X-ray beam impinging from the positive z -axis. Top-left: geometry model and electric potential in 3D. Top-right: cross-section at mid-chamber and equipotential curves. Bottom: electric field component perpendicular to the electrodes at mid-chamber (symmetry plane of the cylinder), as a function of the distance from one of the chamber walls.

Space charge effects stemming from the presence of slowly-drifting ions can modify the electric field, leading to charge losses due to enhanced charge recombination, or to imperfect electron

collection at the anode. For the conditions of our measurements, where the ionization is highly uniform and the external electric field has been established to be uniform within the ionization region, the calculation performed in [31] can be used to assess the situation. In this case, the impact of space charge may be characterized with a single dimensionless parameter α :

$$\alpha = \frac{D}{E_0} \sqrt{\frac{K}{\epsilon\mu}} \quad (\text{A.1})$$

Here D is the conversion gap (0.75 cm), $E_0 = V/D$ is the nominal electric field in the absence of space charge, V the voltage drop between anode and cathode, $\epsilon \simeq \epsilon_0$ the electric permittivity of the medium, μ the positive-ion mobility and K the rate of creation of electron-ion pairs per unit volume. The latter (in units of $[\mu\text{C/s/cm}^3]$) was determined at high electric fields, in conditions of full charge-collection.

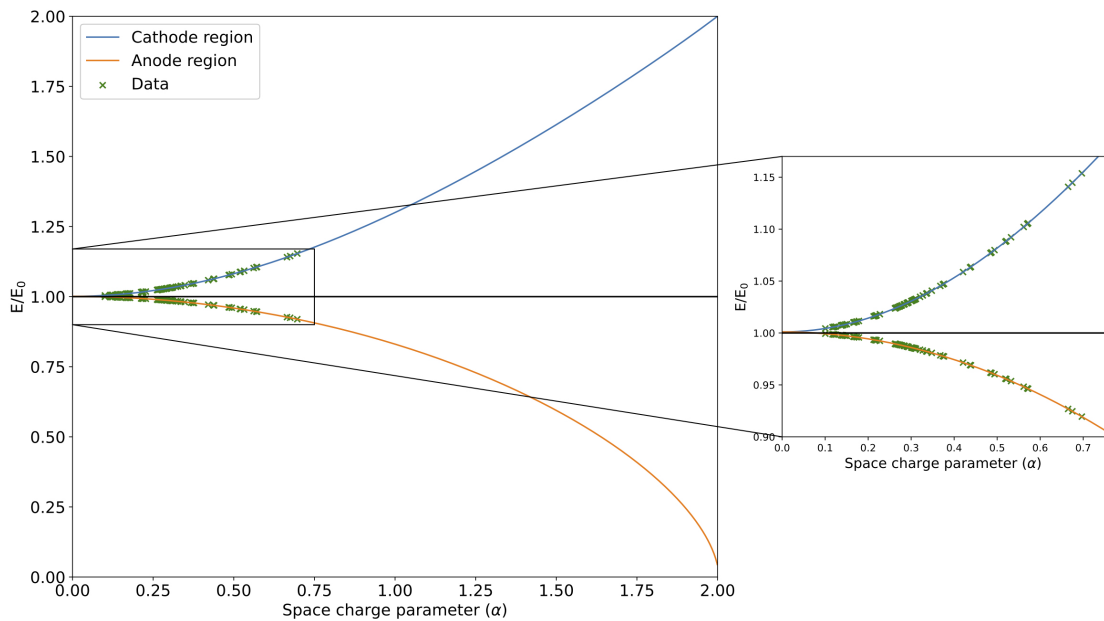
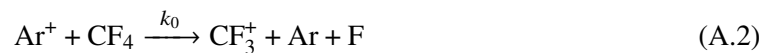


Figure 11. Electric field distortion near cathode/anode as a function of the α parameter (blue/orange lines). Pairs of experimental values obtained in conditions of full charge-collection are overlaid, for all pressures, mixtures and tube intensities employed in this work (crosses).

The input mobilities were obtained in the following way: in argon, the main drifting ions were assumed to be Ar^+ and their mobility taken from [61]. In the case of Ar/CF_4 mixtures and pure CF_4 , CF_3^+ ions were considered instead and their mobility taken from direct measurements in [62]. CF_3^+ ions are produced as a byproduct of dissociation/decay of $\text{CF}_4^{+,*}$ states [41], or through charge transfer reactions with CF_4 [62]:



The electric field has a numerical dependence on α , that can be computed following [31]. As the maximum variations take place close to the anode and cathode, we chose these two cases for representation in Fig. 11, with the experimental conditions corresponding to full charge-collection overlaid (crosses). Based on these results, the field distortions associated to space charge effects are shown to be minimal: values are typically at the $\sim 5\%$ -level or below, with a maximum field distortion of $\sim 15\%$.

B Charge recombination

Electron-ion and ion-ion recombination, either geminal [63], columnar [64] or volume [65] can reduce the collected charge, so it is important to exclude these during measurements. On general grounds, given the relatively low pressures and X-ray energies, the main contribution to charge recombination is expected to come from the volume, and so being associated to the setup geometry and not to the particle type. Therefore any charge recombination present in the system would render the interpretation of the results problematic and must be avoided. During the measurements, the electric field was increased, for any given gas mixture and pressure, up to the point where full charge-collection could be guaranteed, within less than 5% variation relative to the flat-top (see Fig. 2-left for the case of pure CF_4). This already assures that all charge is being collected, except perhaps for stray electrons from diffusion, fringe fields or space charge, effects that are expected to be below 5-10% level as per the discussions in previous sections. The good correlation between ionization rate and tube intensity across all the ionization densities considered (Fig. 2-right) confirms the negligible presence of charge recombination.

For both pure Ar and pure CF_4 , the existence of recombination light at pressures slightly above atmospheric is well documented in case of α -particles [4, 66, 67]: for argon, recombined electron-ion pairs landing in the first p-multiplet yield VUV photons with 100% efficiency; for CF_4 the visible emission is enhanced, yet the detailed pathways are not known. In this latter case, if considering for reference the scintillation yields of pure CF_4 in the 500-800 nm band (796 ph/MeV for α particles [3]) and its W_I value of 34.3 eV/e⁻ [34], the ratio of electrons to photons is about 37. Therefore, even a 2.5% fraction of recombined charge may double the scintillation yields if recombination light would be emitted with 100% probability. It is thus pertinent to study the spectrum of emission for different electric fields and ionization rates. We have chosen for illustration Ar/ CF_4 admixed at 95/5 in Fig. 12, but similar conclusions can be drawn for other admixtures. Besides the large independence observed both with electric field and ionization density, an important additional result is apparent, that has been discussed in the main text in full: wavelength-shifting properties of Ar/ CF_4 mixtures are largely pressure-independent, in the range 1-5 bar.

In order to better understand the absence of charge-recombination effects in our measurements it is possible to resort to previous data, e.g, considering measurements done for α -particles in pure CF_4 at 1 bar [3], for which experimental conditions overlap. The authors reported no recombination light at any electric field in that situation. In our setup the ionization is uniform and volume recombination can be expected to be the main source of charge recombination. When comparing with the conditions in [3], it is thus natural to consider an uniform ionization channel too, with the average ionization and spatial extent of an α particle. We take for simplicity the direction along the field, although this assumption is not critical at the fields discussed (diffusion is largely isotropic). Under the prescribed-diffusion approximation [64], ionization density for α particles

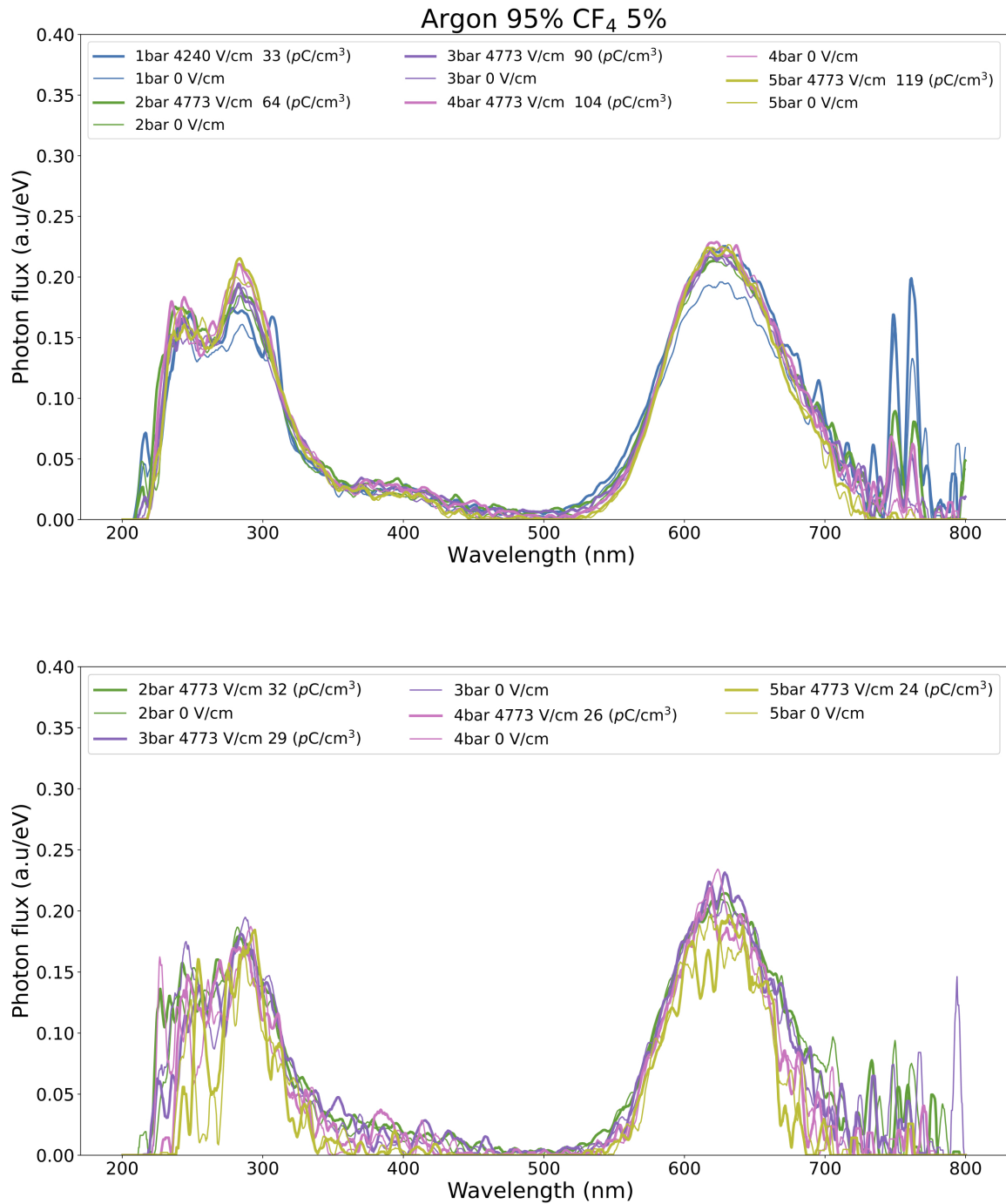


Figure 12. Emission spectra per eV of released energy for Ar/CF₄ admixed at 95/5 and different pressures. Two different electric field conditions are considered: i) zero field and ii) a field sufficient to reach full charge-collection. Top spectra were taken with a tube current of 40 mA while bottom spectra were taken with lower tube currents of 20, 13, 10 and 8 mA, for the same irradiation time.

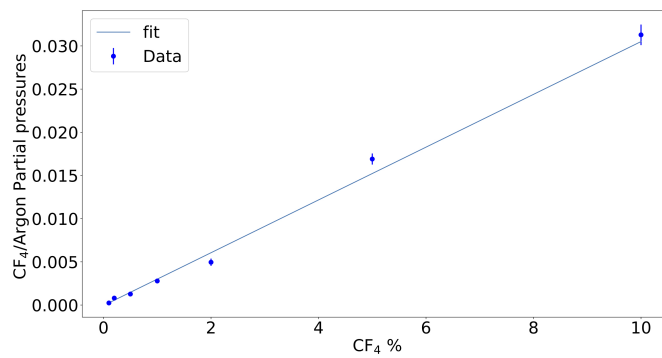
can be approximated by:

$$\left(\frac{dN}{dV}\right)_\alpha = \frac{\varepsilon}{W_I} \frac{n^2}{(\pi R_\alpha D_T^2)} \quad (\text{B.1})$$

where $\varepsilon = 5.5$ MeV is the energy of the α particle, R_α its range at $P_0 = 1$ bar and D_T the transverse diffusion at $P_0 = 1$ bar for the corresponding field. The P -scaling factors are absorbed in the term $n = P/P_0$. Considering $R_\alpha = 1.6$ cm [68] and $D_T = 55 \mu\text{m}/\sqrt{\text{cm}}$ -obtained with Pyboltz for pure CF_4 at 1 bar- and the electric field conditions in [4] (2.2 kV/cm), the average ionization density amounts to ~ 190 pC/cm³. This is 4 times larger than in our 1 bar measurements, and about the maximum levels throughout our work (Fig. 2-right), thus consistent with the fact that no recombination effects are seen in neither case. At 2 bar, where the average ionization density of an α -track in [3] would quadruple the maximum space charge densities explored here, the authors were still able to obtain a recombination-free spectrum upon application of a field of 2.2 kV/cm, comparable to our full-collection field. Conditions corresponding to $P \geq 3$ -5 bar, where recombination became severe in [4] (i.e., full charge-collection not being possible even upon application of fields in the few-kV/cm range), would therefore exceed the ionization densities explored here by a factor of up to 25.

C Gas mixing and calibration

Mixtures were prepared by filling at high CF_4 partial pressure in order to increase the precision of the pressure readings, and diluted then in argon down to low concentrations. The system was left for some time until the concentration displayed by the RGA reached a plateau, moment at which the measurements were conducted. As shown in Fig.13, the pressure ratios of the main CF_4 and argon peaks obtained from the RGA reading show a proportional trend with the target CF_4 concentration estimated from the mixing procedure described above, as expected. Systematic uncertainties due to the resolution of the P -gauge and dilution procedure, and pure statistical uncertainties, were used to calculate the total uncertainty for each data point. A χ^2 -fit to a proportionality law was used on Fig.13 to derive a corrected value for the concentration, with its uncertainty (see adjacent table). Even if, for clarity, the target concentration has been used throughout the text, the experimentally-determined one with its uncertainties will be used in trend plots.



Target Concentration (%)	Calibrated Concentration (%) ± Error
0.1	0.096±0.015
0.2	0.28±0.024
0.5	0.434±0.026
1.0	0.929±0.071
2.0	1.64±0.14
5.0	5.55±0.21
10.0	10.25±0.39

Figure 13. Left: ratio of the partial pressure of CF_4 to argon peaks measured in the RGA during operation, as a function of the target CF_4 concentration. The error bar is estimated from the statistical deviation of measurements performed at different pressures and from systematic uncertainties due to the P -gauge resolution and dilution procedure. Right: target and calibrated concentrations, alongside their uncertainties.